



ELSEVIER

Applied Numerical Mathematics 33 (2000) 71–93



APPLIED
NUMERICAL
MATHEMATICS

www.elsevier.nl/locate/apnum

Computing singular solutions of elliptic boundary value problems in polyhedral domains using the p -FEM

Zohar Yosibash¹

*Pearlstone Center for Aeronautical Engineering Studies, Department of Mechanical Engineering,
Ben-Gurion University of the Negev, Beer-Sheva 84105, Israel*

This paper is dedicated to the memory of Professor Søren Jensen

Abstract

Numerical methods for computing singular solutions of linear second order elliptic partial differential equations (Laplace and Elasticity problems) in polyhedral domains are presented. The singularities may be caused by edges, vertices, or abrupt changes in material properties or boundary conditions. In the vicinity of the singular lines or points the solution can be represented by an asymptotic series, composed of eigen-pairs and their amplitudes. These are of great interest from the point of view of failure initiation because failure theories directly or indirectly involve them.

This paper addresses a general method based on the modified Steklov formulation for computing the eigen-pairs and a dual weak formulation for extracting the amplitudes numerically using the p -version of the finite element method. The methods are post-solution operations on the finite element solution vector and have been shown in a two dimensional setting to be super-convergent. © 2000 IMACS. Published by Elsevier Science B.V. All rights reserved.

Keywords: Singularities; Edge stress intensity functions; p -FEM; Elasticity; Eigen-pairs

1. Introduction and notations

The solution of second order elliptic boundary value problems (BVP) in three-dimensions, in the vicinity of singularities can be decomposed into three different forms, depending whether it is in the neighborhood of an edge, a vertex or an intersection of the edge and the vertex. Mathematical details on the decomposition can be found, e.g., in [1,3,6,8–10] and the references therein. A representative three-dimensional domain denoted by Ω , which contains typical 3-D singularities is shown in Fig 1. Vertex singularities arise in the neighborhood of the vertices A_i , and edge singularities arise in the neighborhood of the edges A_{ij} . *Only straight edges are considered herein* (for curved edges see [6]). Close to the

¹ E-mail: zohary@pversion.bgu.ac.il

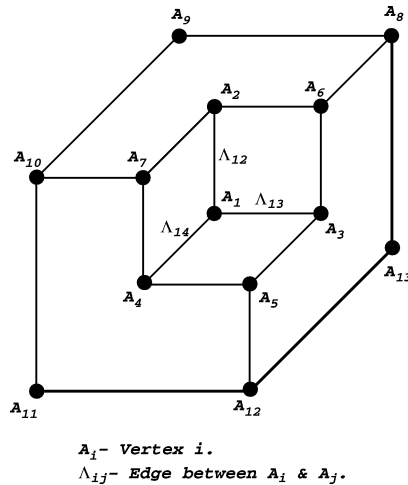


Fig. 1. Typical 3-D singularities.

vertex/edge intersection, the vertex-edge singularities arise. It shall be assumed that curved edges which intersect at vertices do not exist, and that crack faces, if any, lie in a flat plane.

For introductory purposes the simplest elliptic BVP, namely the Laplace equation, is considered:

$$\nabla^2 u = 0 \quad \text{in } \Omega \quad (1)$$

with the following boundary conditions:

$$u = g_1 \quad \text{on } \Gamma_D \subset \partial\Omega, \quad (2)$$

$$\frac{\partial u}{\partial n} = g_2 \quad \text{on } \Gamma_N \subset \partial\Omega, \quad (3)$$

$\Gamma_D \cup \Gamma_N = \partial\Omega$. In the vicinity of edges or vertices of interest, we assume that homogeneous boundary conditions are applied for clarity and simplicity of presentation.

In this section we provide a short outline of the singular solution decomposition in the neighborhood of an edge, a vertex or at a vertex–edge intersection. Based on previous work on two-dimensional singularities, see, e.g., [16,17,22,23], we herein extend the methods developed for singular points shown to be accurate, general and super-convergent, to three-dimensional edge and vertex singularities. Sections 2 and 3 introduce the modified Steklov formulation for extracting edge and vertex eigen-pairs associated with the Laplace operator. In Sections 4 and 5 a more detailed analysis of the modified Steklov method is provided for extracting eigen-pairs associated with edge and vertex elastic singularities. We thereafter introduce the dual weak form for extracting edge flux intensity functions of the Laplace operator in Section 6 as an illustrative example of the required formulation for the elasticity problem. We conclude with a summary in Section 7.

Edge singularities. Let us consider one of the edges denoted by Λ_{ij} connecting the vertices A_i and A_j . Moving away from the vertex a distance $\delta/2$, we create a cylindrical sector sub-domain of radius $r = R$ with the edge Λ_{ij} as its axis. It is denoted by $\mathcal{E}_{\delta,R}(\Lambda_{ij})$, and is shown in Fig. 2 for edge Λ_{12} . It is again emphasized that our attention is restricted to domains having straight edges. The solution in $\mathcal{E}_{\delta,R}$ can be

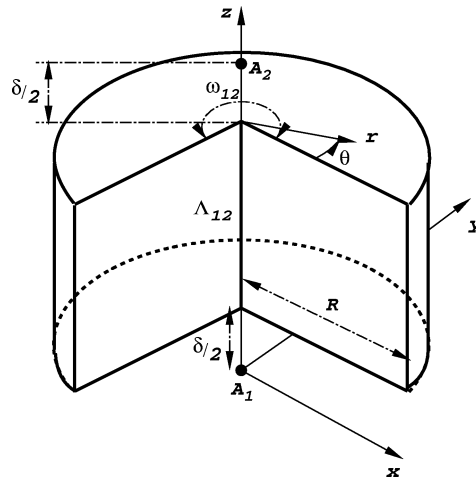


Fig. 2. The edge sub-domain $\mathcal{E}_{\delta,R}(\Lambda_{12})$.

decomposed as follows:

$$u(r, \theta, z) = \sum_{k=1}^K \sum_{s=0}^S a_{ks}(z) r^{\alpha_k} (\ln r)^s f_{ks}(\theta) + v(r, \theta, z), \tag{4}$$

where $S \geq 0$ is an integer which is zero unless α_k is an integer, $\alpha_{k+1} \geq \alpha_k$ are called edge eigen-values, $a_{ks}(z)$ are analytic in z and are denoted by edge flux intensity functions (EFIFs). $f_{ks}(\theta)$ are analytic in θ , called edge eigen-functions. The function $v(r, \theta, z)$ belongs to $H^q(\mathcal{E})$, the usual Sobolev space, where q can be as large as required and depends on K . We shall assume that α_k for $k \leq K$ are not integers, and that no “crossing points” are of interest (see a detailed explanation in [6]), therefore, (4) becomes:

$$u(r, \theta, z) = \sum_{k=1}^K a_k(z) r^{\alpha_k} f_k(\theta) + v(r, \theta, z). \tag{5}$$

Vertex singularities. A sphere of radius $\rho = \delta$, centered in the vertex A_{11} for example, is constructed and intersected with the domain Ω . Then, a cone having an opening angle $\theta = \sigma$ is constructed such that it intersects at A_{11} , and removed from the previously constructed sub-domain, as shown in Fig. 3. The resulting vertex sub-domain is denoted by $\mathcal{V}_\delta(A_{11})$, and the solution u can be decomposed in $\mathcal{V}_\delta(A_{11})$ using a spherical coordinate system by

$$u(\rho, \phi, \theta) = \sum_{l=1}^L \sum_{p=0}^P b_{lp} \rho^{\gamma_l} (\ln \rho)^p h_{lp}(\phi, \theta) + v(\rho, \phi, \theta), \tag{6}$$

where $P \geq 0$ is an integer which is zero unless γ_l is an integer, $\gamma_{l+1} \geq \gamma_l$ are called vertex eigen-values, and $h_{lp}(\phi, \theta)$ are analytic in ϕ and θ away from the edges and are called vertex eigen-functions. b_{lp} are denoted by vertex flux intensity factors (VFIFs). The function $v(r, \theta, z)$ belongs to $H^q(\mathcal{V})$, where q depends on L . We shall assume that γ_l for $l \leq L$ is not an integer, therefore, (6) becomes:

$$u(\rho, \phi, \theta) = \sum_{l=1}^L b_l \rho^{\gamma_l} h_l(\phi, \theta) + v(\rho, \phi, \theta). \tag{7}$$

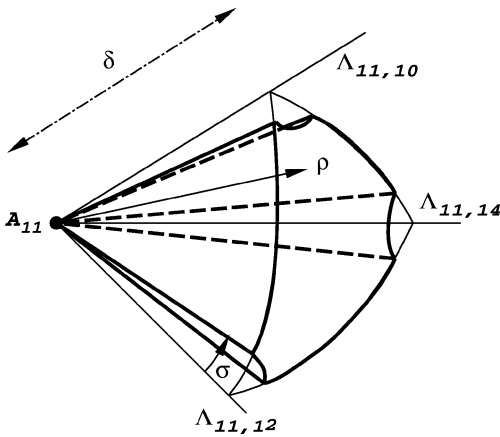


Fig. 3. The vertex neighborhood $\mathcal{V}_\delta(A_{11})$.

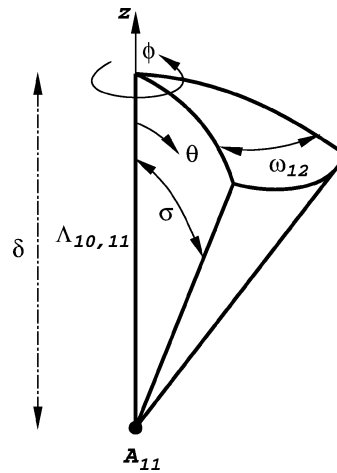


Fig. 4. The vertex–edge neighborhood $\mathcal{V}E_{\delta,R}(A_{11}, \Lambda_{10,11})$.

Vertex–edge singularities. The most complicated decomposition of the solution arises in case of a vertex–edge intersection, but this will not be addressed herein. Only a short outline is provided. For example, let us consider the neighborhood where the edge $\Lambda_{10,11}$ approaches the vertex A_{11} . A spherical coordinate system is located in the vertex A_{11} , and a cone having an opening angle $\theta = \sigma$ with its vertex coinciding with A_{11} is constructed with $\Lambda_{10,11}$ being its center-axis. This cone is terminated by a ball-shaped basis having a radius $\rho = \delta$, as shown in Fig. 4. The resulting vertex–edge sub-domain is denoted by $\mathcal{V}E_{\delta,R}(A_{11}, \Lambda_{10,11})$, and the solution u can be decomposed in $\mathcal{V}E_{\delta,R}(A_{11}, \Lambda_{10,11})$:

$$\begin{aligned}
 u(\rho, \phi, \theta) = & \sum_{k=1}^K \sum_{s=0}^S \left(\sum_{l=1}^L a_{ksl} \rho^{\gamma_l} + m_{ks}(\rho) \right) (\sin \theta)^{\alpha_k} [\ln(\sin \theta)]^s g_{ks}(\phi) \\
 & + \sum_{l=1}^L \sum_{p=0}^P c_{lp} \rho^{\gamma_l} (\ln \rho)^p h_{lp}(\phi, \theta) + v(\rho, \phi, \theta),
 \end{aligned} \tag{8}$$

where $m_{ks}(\rho)$ are analytic in ρ , $g_{ks}(\phi)$ are analytic in ϕ and $h_{lp}(\phi, \theta)$ are analytic in ϕ and θ . The function $v(r, \theta, z)$ belongs to $H^q(\mathcal{V}E)$ where q is as large as required depending on L and K .

The eigen-values and the eigen-functions are associated pairs (eigen-pairs) which depend on the material properties, the geometry, and the boundary conditions *in the vicinity of the singular vertex/edge only*. Similarly, the solution for problems in linear elasticity, in the neighborhood of singular vertices/edges is analogous to (4)–(8), the differences are that the equations are in a vector form and the eigen-pairs may be complex. For general singular points the exact solution u_{EX} is generally not known explicitly, i.e., neither the exact eigen-pairs nor the exact EFIFs, VFIFs are known, therefore numerical approximations are sought.

2. Computing edge eigen-pairs for the Laplace problem

For the Laplace equation, we may perform a separation of variables procedure in the neighborhood of the edge singularity as shown in (5). Each eigen-pair (the n th, for example, $r^{\alpha_n} f_n(\theta)$) is independent

of z and satisfies the Laplace equation over the plane (r, θ) which is perpendicular to the edge. *This is exactly a 2-D problem and the eigen-pairs are identical to the 2-D eigen-pairs* (see for detailed mathematical analysis [9, Chapter 2.5]). Thus, the modified Steklov method described in [22] can be used for determining the eigen-pairs in the neighborhood of edge singularities on a two-dimensional plane perpendicular to the edge.

Remark 1. Of course, eigen-pairs for the Laplace operator are known explicitly, but for multi-material interface problems of general scalar elliptic operators (provided that in the z direction the domain remains isotropic) one has to use numerical methods to compute the eigen-pairs as the modified Steklov formulation.

3. Computing vertex eigen-pairs for the Laplace problem

Based on the methods documented in [3,22], we herein provide the modified Steklov formulation for the computation of vertex eigen-pairs. Consider the sub-domain shown in Fig. 5 in the vicinity of a vertex. Edge singularities exist along the edges $\Lambda_{11,12}$, $\Lambda_{11,14}$ and $\Lambda_{11,10}$, so that proper numerical treatment is required in their vicinity. A possibility to overcome the deterioration of the numerical approximations due to the vertex–edge singularities is to use the Auxiliary Mapping Method [10], having in hand already the edge eigen-values, or to enrich the finite element space with edge-singular shape functions in the elements adjacent to the edges. If neither methods are used, one has to geometrically refine the mesh in the vicinity of the edges. Based on (7), in the neighborhood of the vertex, $u \propto \rho^\gamma h(\phi, \theta)$, therefore on the sphere-shaped boundary, $\rho = P$, for example, we have

$$\frac{\partial u}{\partial n} = \frac{\partial u}{\partial \rho} = \frac{\gamma}{P} u \quad \text{on } \rho = P. \tag{9}$$

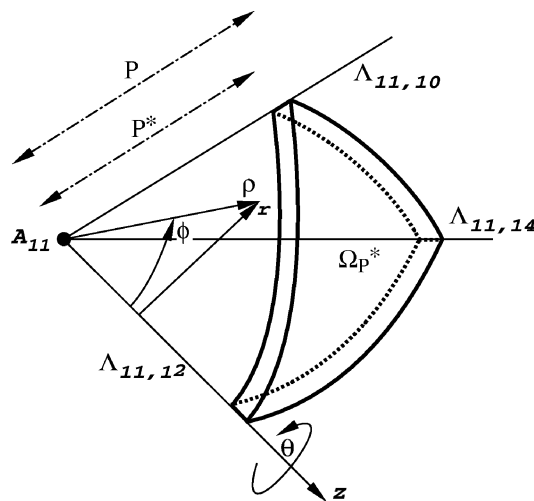


Fig. 5. Domain for vertex eigen-pairs extraction.

Assume that homogeneous Neumann boundary conditions are prescribed in the vicinity of the vertex, thus we have to solve over Ω_p^* the following classical eigen-value problem:

$$\begin{aligned} \nabla^2 u &= 0 && \text{in } \Omega_p^*, \\ \frac{\partial u}{\partial n} &= 0 && \text{on } \Gamma_N, \\ \frac{\partial u}{\partial \rho} - \frac{\gamma}{P} u &= 0 && \text{on } \rho = P, \\ \frac{\partial u}{\partial \rho} - \frac{\gamma}{P^*} u &= 0 && \text{on } \rho = P^*, \end{aligned} \quad (10)$$

where Γ_N for this case are the plane boundaries of Ω_p^* shown in Fig. 5. The weak eigen-formulation associated with (10) is obtained by following the steps presented in [22]:

- **Seek** $\gamma \in \mathcal{C}$, $0 \neq u \in H^1(\Omega_p^*)$, such that

$$\mathcal{B}(u, v) = \gamma [\mathcal{M}_P(u, v) + \mathcal{M}_{P^*}(u, v)], \quad \forall v \in H^1(\Omega_p^*), \quad (11)$$

where:

$$\mathcal{B}(u, v) \triangleq \iiint_{\Omega_p^*} \nabla u \cdot \nabla v \rho^2 \sin \phi \, d\rho \, d\phi \, d\theta,$$

$$\mathcal{M}_P(u, v) = P \iint_{\phi, \theta} [uv \sin \phi]_{\rho=P} \, d\phi \, d\theta, \quad (12)$$

$$\mathcal{M}_{P^*}(u, v) = P^* \iint_{\phi, \theta} [uv \sin \phi]_{\rho=P^*} \, d\phi \, d\theta. \quad (13)$$

The weak formulation (11) may be solved by the p -version of the finite element method through a meshing process, dividing the domain Ω_p^* into 3-D hexahedra/tetrahedral elements. It has to be emphasized that although the vertex singularity has been removed from the domain Ω_p^* , yet edge singularities may be present.

4. Computing edge eigen-pairs for the elasticity problem

The elastostatic displacements field in three-dimensions, $\mathbf{u} = (u_x, u_y, u_z)^T$, in the vicinity of an edge can be decomposed in terms of edge eigen-pairs and edge stress intensity functions (ESIFs). Mathematical details on the decomposition can be found, e.g., in [1,8,9] and the references therein. Elastic edge singularities have been less investigated, especially when associated with anisotropic materials and multi-material interfaces. Analytical methods as in [18,19] provide the means for computing the eigen-pairs for a two-material interface however requires extensive mathematics. Several numerical methods, have been suggested lately. Among them [5,7,11,12,14] and the references therein.

In the neighborhood of a typical edge (for example, $\mathcal{E}_{\delta,R}$), the displacement field can be decomposed as follows:

$$\mathbf{u}(r, \theta, z) = \sum_{k=1}^K \sum_{s=0}^S a_{ks}(z) r^{\alpha_k} (\ln r)^s \mathbf{f}_{ks}(\theta) + \mathbf{w}(r, \theta, z), \quad (14)$$

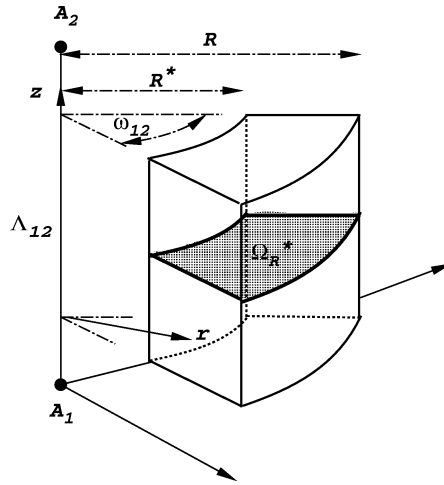


Fig. 6. The modified Steklov domain Ω_R^* .

where $S \geq 0$ is an integer which is zero for most practical problems, except for special cases, and $a_{ks}(z)$ are analytic in z called edge stress intensity functions (ESIFs). The vector function $\mathbf{w}(r, \theta, z)$ belongs to $[H^q(\mathcal{E}_{\delta,R})]^3$, where q depends on K . We shall address herein only these cases where $S = 0$, therefore, (14) becomes:

$$\mathbf{u}(r, \theta, z) = \sum_{k=1}^K a_k(z)r^{\alpha_k} \mathbf{f}_k(\theta) + \mathbf{w}(r, \theta, z). \tag{15}$$

We denote the tractions on the boundaries by $\mathbf{T} = (T_x \ T_y \ T_z)^T$, and the Cartesian stress vector by $\boldsymbol{\sigma} = (\sigma_x \ \sigma_y \ \sigma_z \ \tau_{xy} \ \tau_{yz} \ \tau_{xz})^T$. In the vicinity of the edge we assume that no body forces are present.

For computing eigen-pairs, a *two-dimensional* sub-domain Ω_R^* is constructed in a plane perpendicular to the edge (z -axis) and bounded by the radii $r = R^*$ and $r = R$, as shown in Fig. 6.

On the boundaries $\theta = 0$ and $\theta = \omega_{ij}$ of the sub-domain Ω_R^* either homogeneous traction boundary conditions ($\mathbf{T} = \mathbf{0}$), or homogeneous displacements boundary conditions, or a combinations of these are prescribed.

In view of (15), \mathbf{u} in Ω_{R^*} (respectively \mathbf{v}) has the functional representation

$$\mathbf{u} \stackrel{\text{def}}{=} a(z)r^\alpha (f_x(\theta), f_y(\theta), f_z(\theta))^T = a(z)r^\alpha \mathbf{f}(\theta), \quad \mathbf{v} \stackrel{\text{def}}{=} b(z)r^\alpha \mathbf{f}(\theta). \tag{16}$$

We also denote the *in-plane* variation of the displacements as follows:

$$\tilde{\mathbf{u}}(r, \theta) \stackrel{\text{def}}{=} \frac{\mathbf{u}}{a(z)}, \quad \tilde{\mathbf{v}}(r, \theta) \stackrel{\text{def}}{=} \frac{\mathbf{v}}{b(z)}. \tag{17}$$

Following the steps presented in detail in [20], an eigen-problem is cast in a weak form which is an integral equation (modified Steklov weak form) over a two dimensional domain involving the three displacements field.

- **Seek** $\alpha \in \mathbb{C}$, $\mathbf{0} \neq \tilde{\mathbf{u}} \in [H^1(\Omega_R^*)]^3$, such that $\forall \tilde{\mathbf{v}} \in [H^1(\Omega_R^*)]^3$,

$$\mathcal{B}(\tilde{\mathbf{u}}, \tilde{\mathbf{v}}) - [\mathcal{N}_R(\tilde{\mathbf{u}}, \tilde{\mathbf{v}}) - \mathcal{N}_{R^*}(\tilde{\mathbf{u}}, \tilde{\mathbf{v}})] = \alpha [\mathcal{M}_R(\tilde{\mathbf{u}}, \tilde{\mathbf{v}}) - \mathcal{M}_{R^*}(\tilde{\mathbf{u}}, \tilde{\mathbf{v}})] \tag{18}$$

with

$$\mathcal{B}(\tilde{\mathbf{u}}, \tilde{\mathbf{v}}) \stackrel{\text{def}}{=} \int_{R^*}^R \int_0^{\omega_{12}} \left\{ \left([A_r] \partial_r + [A_\theta] \frac{\partial_\theta}{r} \right) \tilde{\mathbf{v}} \right\}^T [E] \left\{ \left([A_r] \partial_r + [A_\theta] \frac{\partial_\theta}{r} \right) \tilde{\mathbf{u}} \right\} r \, d\theta \, dr, \quad (19)$$

$$\mathcal{N}_R(\tilde{\mathbf{u}}, \tilde{\mathbf{v}}) \stackrel{\text{def}}{=} \int_0^{\omega_{12}} \tilde{\mathbf{v}}^T [A_r]^T [E] [A_\theta] \partial_\theta \tilde{\mathbf{u}}|_{r=R} \, d\theta, \quad (20)$$

$$\mathcal{M}_R(\tilde{\mathbf{u}}, \tilde{\mathbf{v}}) \stackrel{\text{def}}{=} \int_0^{\omega_{12}} \tilde{\mathbf{v}}^T [A_r]^T [E] [A_r] \tilde{\mathbf{u}}|_{r=R} \, d\theta, \quad (21)$$

where

$$[A_r] \stackrel{\text{def}}{=} \begin{bmatrix} \cos \theta & 0 & 0 \\ 0 & \sin \theta & 0 \\ 0 & 0 & 0 \\ \sin \theta & \cos \theta & 0 \\ 0 & 0 & \sin \theta \\ 0 & 0 & \cos \theta \end{bmatrix}, \quad [A_\theta] \stackrel{\text{def}}{=} \begin{bmatrix} -\sin \theta & 0 & 0 \\ 0 & \cos \theta & 0 \\ 0 & 0 & 0 \\ \cos \theta & -\sin \theta & 0 \\ 0 & 0 & \cos \theta \\ 0 & 0 & -\sin \theta \end{bmatrix} \quad (22)$$

and $[E]$ is the material matrix given in (36).

Remark 2. Although both $\tilde{\mathbf{u}}$ and $\tilde{\mathbf{v}}$ have three components, the domain over which the weak eigen-formulation is defined is two-dimensional, and excludes any singular points. Therefore, the application of the p -version of the FEM for solving (18) is expected to be very efficient.

Remark 3. The bilinear forms \mathcal{N}_R and \mathcal{N}_{R^*} are *non-symmetric* with respect to $\tilde{\mathbf{u}}$ and $\tilde{\mathbf{v}}$, thus are not self-adjoint. As a consequence, the “minimax principle” does not hold, and any approximation of the eigenvalues (obtained using a finite dimension subspace of $[H^1(\Omega_R^*)]^3$) cannot be considered as an upper bound of the exact ones and the monotonic convergence as the sub-space is enriched is lost as well. Nevertheless, convergence is assured (with a very high rate as will be shown by the numerical examples) under a general proof provided in [2].

Remark 4. Note that in (18) we do not limit the domain Ω_R^* to be isotropic, and in fact (18) can be applied to multi-material anisotropic interface.

Remark 5. When homogeneous displacement boundary conditions are applied, one has to restrict the spaces to $[H_0^1(\Omega_R^*)]^3$, or a variation of it, so as to apply the essential boundary condition restrictions on the spaces in which $\tilde{\mathbf{u}}$ and $\tilde{\mathbf{v}}$ lay.

4.1. Numerical treatment by the finite element method

We provide herein a short outline on the discretization of the weak eigen-formulation (18) by the p -version of the finite element method. Details and explicit expressions can be found in [20].

Assume that the domain Ω_R^* consists of three different material as shown in Fig. 7. We divided Ω_R^* into, let us say, 3 finite elements, through a meshing process. Let us consider a typical element, element number 1, shown in Fig. 7, bounded by $\theta_1 \leq \theta \leq \theta_2$. A standard element in the ξ, η plane such that

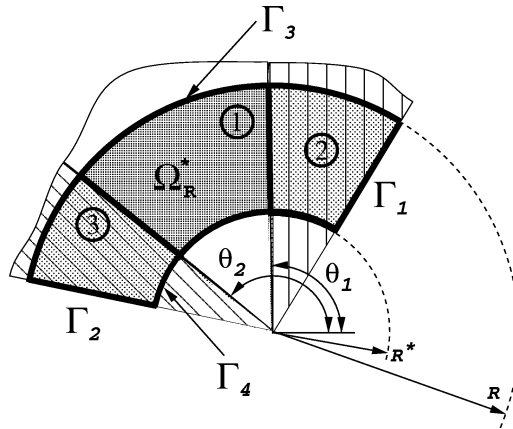


Fig. 7. A typical finite element in the domain Ω_R^* .

$-1 < \xi < 1, -1 < \eta < 1$ is considered, over which the polynomial basis and trial functions are defined. These standard elements are then mapped by appropriate mapping functions onto the “real” elements (for details see [15, Chapters 5, 6]). The functions $\tilde{u}_x, \tilde{u}_y, \tilde{u}_z$ are expressed in terms of the basis functions $\Phi_i(\xi, \eta)$ in the standard plane:

$$\tilde{\mathbf{u}} = \begin{bmatrix} \Phi_1 & \dots & \Phi_N & 0 & \dots & 0 & 0 & \dots & 0 \\ 0 & \dots & 0 & \Phi_1 & \dots & \Phi_N & 0 & \dots & 0 \\ 0 & \dots & 0 & 0 & \dots & 0 & \Phi_1 & \dots & \Phi_N \end{bmatrix} \begin{Bmatrix} c_1 \\ \vdots \\ c_{3N} \end{Bmatrix} \stackrel{\text{def}}{=} [\Phi] \mathbf{C}, \tag{23}$$

where c_i are the amplitudes of the basis functions. Similarly, $\tilde{\mathbf{v}} \stackrel{\text{def}}{=} [\Phi] \mathbf{B}$.

The unconstrained stiffness matrix corresponding to $\mathcal{B}(\tilde{\mathbf{u}}, \tilde{\mathbf{v}})$ on the typical element is given by

$$[K] \stackrel{\text{def}}{=} \int_{R^*} \int_{\theta_1}^{\theta_2} \left\{ \left([A_r] \partial_r + [A_\theta] \frac{\partial_\theta}{r} \right) [\Phi] \right\}^T [E] \left\{ \left([A_r] \partial_r + [A_\theta] \frac{\partial_\theta}{r} \right) [\Phi] \right\} r \, d\theta \, dr. \tag{24}$$

The matrices corresponding to \mathcal{M}_R and \mathcal{N}_R on a typical element are computed according to

$$\mathcal{N}_R(\tilde{\mathbf{u}}, \tilde{\mathbf{v}}) = \mathbf{B}^T \left(\int_{-1}^1 [\tilde{P}]^T [E] [\partial P] |_{\eta=-1} \, d\xi \right) \mathbf{C} \stackrel{\text{def}}{=} \mathbf{B}^T [N_R] \mathbf{C}, \tag{25}$$

$$\mathcal{M}_R(\tilde{\mathbf{u}}, \tilde{\mathbf{v}}) = \mathbf{B}^T \left(\frac{\theta_2 - \theta_1}{2} \int_{-1}^1 [\tilde{P}]^T [E] [\tilde{P}] |_{\eta=-1} \, d\xi \right) \mathbf{C} \stackrel{\text{def}}{=} \mathbf{B}^T [M_R] \mathbf{C} \tag{26}$$

with $[\tilde{P}]$ and $[\partial P]$ explicitly given in [20].

The matrices $[N_{R^*}]$ and $[M_{R^*}]$ have same values as those of $[N_R]$ and $[M_R]$, but of opposite sign. Denoting the set of amplitudes of the basis functions associated with the artificial boundary Γ_3 by \mathbf{C}_R , and those associated with the artificial boundary Γ_4 by \mathbf{C}_{R^*} , the eigen-pairs can be obtained by solving

the generalized matrix eigen-problem:

$$[K]C - ([N_R]C_R - [N_{R^*}]C_{R^*}) = \alpha([M_R]C_R - [M_{R^*}]C_{R^*}). \quad (27)$$

Augmenting the coefficients of the basis functions associated with Γ_3 with those associated with Γ_4 , and denoting them by the vector C_{RR^*} , (27) becomes

$$[K]C - [N_{RR^*}]C_{RR^*} = \alpha[M_{RR^*}]C_{RR^*}. \quad (28)$$

We assemble the left-hand part of (28). The vector which represents the total number of nodal values in Ω_R^* may be divided into two vectors such that one contains the coefficients C_{RR^*} , and the other contains the remaining coefficients: $C^T = \{C_{RR^*}^T, C_{in}^T\}$. By partitioning $[K]$, we can write the eigen-problem (28) in the form

$$\begin{bmatrix} [K] - [N_{RR^*}] & [K_{RR^*-in}] \\ [K_{in-RR^*}] & [K_{in}] \end{bmatrix} \begin{Bmatrix} C_{RR^*} \\ C_{in} \end{Bmatrix} = \alpha \begin{bmatrix} [M_{RR^*}] & [0] \\ [0] & [0] \end{bmatrix} \begin{Bmatrix} C_{RR^*} \\ C_{in} \end{Bmatrix}. \quad (29)$$

The relation in (29) can be used to eliminate C_{in} by static condensation, thus obtaining the reduced eigen-problem

$$[K_S]C_{RR^*} = \alpha[M_{RR^*}]C_{RR^*}, \quad (30)$$

where

$$[K_S] = ([K] - [N_{RR^*}]) - [K_{RR^*-in}][K_{in}]^{-1}[K_{in-RR^*}].$$

For the solution of the eigen-problem (30), it is important to note that $[K_S]$ is, in general, a full matrix. However, since the order of the matrices is relatively small, the solution (using Cholesky factorization to compute $[K_{in}]^{-1}$) is not expensive.

Remark 6. There is the possibility that m multiple eigenvalues exist with less than m corresponding eigenvectors (the algebraic multiplicity is higher than the geometric multiplicity). This is associated with the special cases when the asymptotic expansion contains power-logarithmic terms, and this behavior triggers the existence of $\ln(r)$ terms.

Remark 7. Although we derived our matrices as if only one finite element exists along the boundary Γ_3 and Γ_4 , the formulation for multiple finite elements is identical, and the matrices $[K]$, $[N_R]$ and $[M_R]$ are obtained by an assembly procedure.

4.2. Numerical example: Two cross-ply anisotropic laminate

As an example, we study edge singularities associated with a two cross-ply anisotropic laminate. Consider a composite laminate with ply properties typical of a high-modulus graphite-epoxy system, as shown in Fig. 8. The orientation of fibers differs from layer to layer. Referring to the principle direction of the fibers, we define

$$\begin{aligned} E_L &= 1.38 \times 10^5 \text{ MPa} (20 \times 10^6 \text{ psi}), & E_T &= E_z = 1.45 \times 10^4 \text{ MPa} (2.1 \times 10^6 \text{ psi}), \\ G_{LT} &= G_{Lz} = G_{Tz} = 0.586 \times 10^4 \text{ MPa} (0.85 \times 10^6 \text{ psi}), & \nu_{LT} &= \nu_{Lz} = \nu_{Tz} = 0.21, \end{aligned}$$

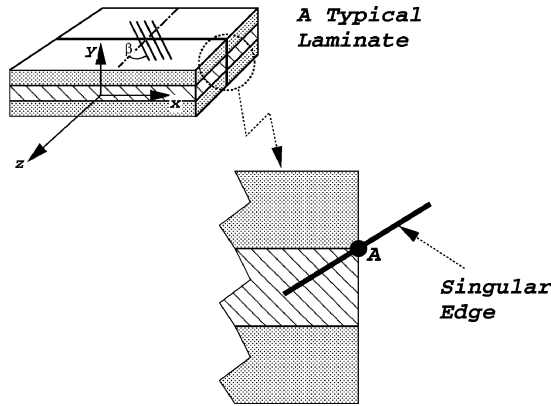


Fig. 8. Cross-ply anisotropic laminate.

where the subscripts L, T, z refer to fiber, transverse and thickness directions of an individual ply, respectively. The material matrix $[E]$ for a ply with fibers orientation rotated by an angle β about the y -axis is given by

$$[E] = [T(\beta)]^T [E_o] [T(\beta)], \tag{31}$$

where

$$[T(\beta)] = \begin{pmatrix} c^2 & 0 & s^2 & 0 & 0 & c \cdot s \\ 0 & 1 & 0 & 0 & 0 & 0 \\ s^2 & 0 & c^2 & 0 & 0 & -c \cdot s \\ 0 & 0 & 0 & c & s & 0 \\ 0 & 0 & 0 & -s & c & 0 \\ -2c \cdot s & 0 & 2c \cdot s & 0 & 0 & c^2 - s^2 \end{pmatrix}, \quad c \stackrel{\text{def}}{=} \cos(\beta), \quad s \stackrel{\text{def}}{=} \sin(\beta).$$

The material matrix in the L, T, z “ply coordinate system” is given by

$$[E_o] = V \begin{pmatrix} (1 - \nu_{Tz}\nu_{zT})E_L & (\nu_{LT} + \nu_{Lz}\nu_{zT})E_T & (\nu_{zL} + \nu_{zT}\nu_{TL})E_L & 0 & 0 & 0 \\ & (1 - \nu_{Lz}\nu_{zL})E_T & (\nu_{zT} + \nu_{LT}\nu_{zL})E_T & 0 & 0 & 0 \\ & & (1 - \nu_{LT}\nu_{TL})E_z & 0 & 0 & 0 \\ & & & \frac{G_{LT}}{V} & 0 & 0 \\ & & & & \frac{G_{Tz}}{V} & 0 \\ & & & & & \frac{G_{Lz}}{V} \end{pmatrix}, \tag{32}$$

$$V \stackrel{\text{def}}{=} (1 - \nu_{LT}\nu_{TL} - \nu_{Tz}\nu_{zT} - \nu_{Lz}\nu_{zL} - 2\nu_{LT}\nu_{Tz}\nu_{zL})^{-1},$$

$$\nu_{TL} = \nu_{LT} \frac{E_T}{E_L}, \quad \nu_{zT} = \nu_{Tz} \frac{E_z}{E_T}, \quad \nu_{zL} = \nu_{Lz} \frac{E_z}{E_L}.$$

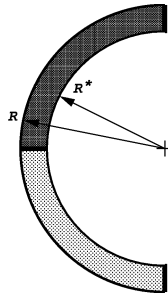


Fig. 9. Finite element mesh used for the cross-ply anisotropic laminate.

However, the L, T, z “ply coordinates” do not match the x, y, z coordinate system shown in Fig. 8, so one has to associate the L ply direction with coordinate z , the T ply direction with coordinate x and the z ply direction with coordinate y . Thus, in order to use (31), one has to change rows and columns in the matrix $[E_o]$, resulting with

$$[E_o] = V \begin{pmatrix} (1 - \nu_{Lz}\nu_{zL})E_T & (\nu_{zT} + \nu_{LT}\nu_{zL})E_T & (\nu_{LT} + \nu_{Lz}\nu_{zT})E_T & 0 & 0 & 0 \\ & (1 - \nu_{LT}\nu_{TL})E_z & (\nu_{zL} + \nu_{zT}\nu_{TL})E_L & 0 & 0 & 0 \\ & & (1 - \nu_{Tz}\nu_{zT})E_L & 0 & 0 & 0 \\ & & & \frac{G_{Tz}}{V} & 0 & 0 \\ & & & & \frac{G_{Lz}}{V} & 0 \\ & & & & & \frac{G_{LT}}{V} \end{pmatrix}. \quad (33)$$

Note that the angle β in Fig. 8 has a negative sign when used with (31).

We investigate the eigen-pairs associated with the singularities near the junction of the free edge and the interface, for a commonly used $[\pm\beta]$ angle-ply composite. Of course, the eigen-pairs depend on β and we chose $\beta = 45^\circ$ for which the first 12 exact non-integer eigen-pairs are reported in [19] with 8 decimal significant digits: $\alpha_1 = 0.974424342$, $\alpha_{2,3} = 1.88147184 \pm i0.23400497$, $\alpha_{4,5} = 2.5115263 \pm i0.79281732 \dots$

The two-element mesh shown in Fig. 9 is used in our computation. The rate of convergence of the eigen-values is clearly visible when plotted on a log-log scale as shown in Fig. 10. The eigen-function vector (displacement fields) associated with α_1 obtained at $p = 8$ is illustrated in Fig. 11.

The variation of the eigen-values for different $[\pm\beta]$ cross-ply laminate and many more other example problems are provided in [21].

5. Vertex singularities for elasticity problem

Let us assume that the three-dimensional domain Ω has a rotationally symmetric conical vertex O on its boundary as shown in Fig. 12 with $\theta_o \in (0, \pi)$. The solution to the linear elastic problem in the neighborhood of the vertex O is naturally expressed in terms of the spherical coordinates ρ, ϕ, θ , with

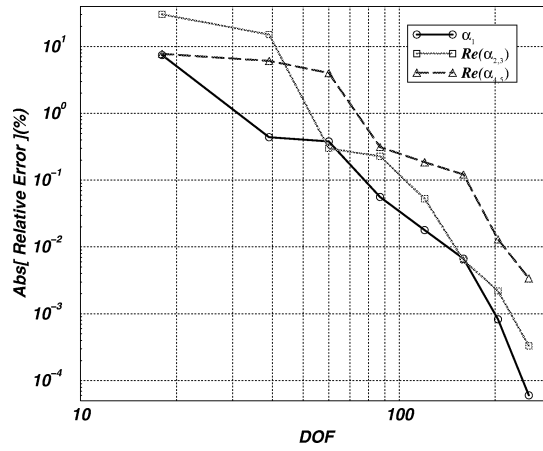


Fig. 10. Convergence of edge eigen-values for the cross-ply anisotropic laminate.

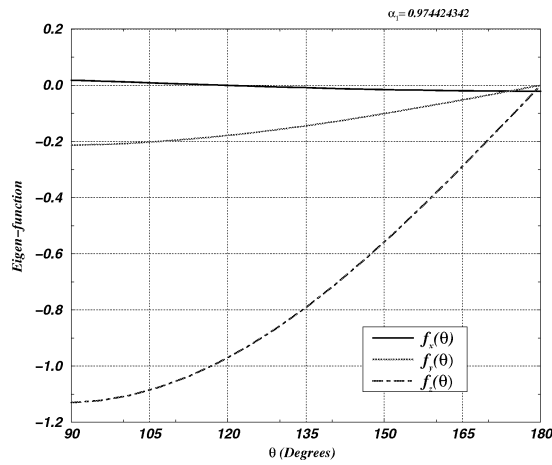


Fig. 11. Edge eigen-functions associated with α_1 for the cross-ply anisotropic laminate.

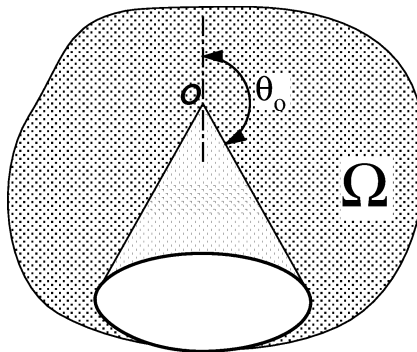


Fig. 12. Typical 3-D domain with a rotationally symmetric conical vertex.

the origin at the vertex O ($0 \leq \rho, 0 \leq \phi < 2\pi, 0 < \theta < \pi$). In the vicinity of O the displacements field can be represented as follows (see, e.g., [4]):

$$\begin{Bmatrix} u_x \\ u_y \\ u_z \end{Bmatrix} \stackrel{\text{def}}{=} \mathbf{u}(\rho, \theta, \phi) = \sum_{k=1}^K \sum_{s=0}^S a_{ks} \rho^{\alpha_k} (\ln \rho)^s \mathbf{f}_{ks}(\theta, \phi) + \mathbf{w}(\rho, \theta, \phi), \tag{34}$$

where $\mathbf{w} \in [H^q(\Omega)]^3$, q being as large as desired and depends on K .

The stress-displacements relationship through the constitutive material law (Hooke’s law) is given by

$$\boldsymbol{\sigma} = [E][D]\mathbf{u} \tag{35}$$

with $[D]$ and $[E]$ (material matrix):

$$[D] \stackrel{\text{def}}{=} \begin{bmatrix} \partial_x & 0 & 0 \\ 0 & \partial_y & 0 \\ 0 & 0 & \partial_z \\ \partial_y & \partial_x & 0 \\ 0 & \partial_z & \partial_y \\ \partial_z & 0 & \partial_x \end{bmatrix}, \quad \begin{cases} \partial_x \stackrel{\text{def}}{=} \frac{\partial}{\partial x} \\ \partial_y \stackrel{\text{def}}{=} \frac{\partial}{\partial y} \\ \partial_z \stackrel{\text{def}}{=} \frac{\partial}{\partial z} \end{cases}, \quad [E] = \begin{bmatrix} E_1 & E_2 & E_4 & E_7 & E_{11} & E_{16} \\ & E_3 & E_5 & E_8 & E_{12} & E_{17} \\ & & E_6 & E_9 & E_{13} & E_{18} \\ & & & E_{10} & E_{14} & E_{19} \\ & & & & E_{15} & E_{20} \\ & & & & & E_{21} \end{bmatrix}. \tag{36}$$

The Navier–Lamé second-order differential equations (equilibrium equations in terms of the displacements) can be cast in a weak form:

- Seek $\mathbf{u} \in [H^1(\Omega)]^3$, such that

$$\mathcal{B}(\mathbf{u}, \mathbf{v}) = \mathcal{F}(\mathbf{v}) \quad \forall \mathbf{v} \in [H^1(\Omega)]^3, \tag{37}$$

where

$$\mathcal{B}(\mathbf{u}, \mathbf{v}) \stackrel{\text{def}}{=} \iiint_{\Omega} ([D]\mathbf{v})^T [E][D]\mathbf{u} \, dV, \tag{38}$$

$$\mathcal{F}(\mathbf{v}) \stackrel{\text{def}}{=} \iint_{\partial\Omega} (\mathbf{v})^T \mathbf{T} \, dA. \tag{39}$$

If homogeneous displacement boundary conditions are prescribed on the boundary of the domain $\partial\Omega$, then the weak form (37) remains unchanged except for the spaces in which \mathbf{u} and \mathbf{v} lie.

We introduce the outward normal vector $\mathbf{n} = (n_x n_y n_z)^T$ on a spherical surface:

$$\mathbf{n} = (\sin \theta \cos \phi, \sin \theta \sin \phi, \cos \theta)^T$$

so that the traction vector \mathbf{T} can be expressed by

$$\mathbf{T} = \underbrace{\begin{bmatrix} n_x & 0 & 0 & n_y & 0 & n_z \\ 0 & n_y & 0 & n_x & n_z & 0 \\ 0 & 0 & n_z & 0 & n_y & n_x \end{bmatrix}}_{[n]} \boldsymbol{\sigma}. \tag{40}$$

Any displacement field of the form $\mathbf{u} = \rho^\alpha \mathbf{f}(\phi, \theta)$ satisfies the Navier–Lame equilibrium equations in the neighborhood of the vertex. With the above notation, the differential operator $[D]$ acting on \mathbf{u} of the above form can be decomposed as follows:

$$[D]\mathbf{u} = \frac{1}{\rho} (\alpha [n]^T + [D^{(\theta, \phi)}]) \mathbf{u}, \tag{41}$$

where

$$[D^{(\theta,\phi)}] = \begin{bmatrix} \cos \theta \cos \phi \partial_\theta - \frac{\sin \phi}{\sin \theta} \partial_\phi & 0 & 0 \\ 0 & \cos \theta \sin \phi \partial_\theta + \frac{\cos \phi}{\sin \theta} \partial_\phi & 0 \\ 0 & 0 & -\sin \theta \partial_\theta \\ \cos \theta \sin \phi \partial_\theta + \frac{\cos \phi}{\sin \theta} \partial_\phi & \cos \theta \cos \phi \partial_\theta - \frac{\sin \phi}{\sin \theta} \partial_\phi & 0 \\ 0 & -\sin \theta \partial_\theta & \cos \theta \sin \phi \partial_\theta + \frac{\cos \phi}{\sin \theta} \partial_\phi \\ -\sin \theta \partial_\theta & 0 & \cos \theta \cos \phi \partial_\theta - \frac{\sin \phi}{\sin \theta} \partial_\phi \end{bmatrix}.$$

Consider the sub-domain Ω^* in the neighborhood of the conical point of interest, bounded by a cone (which is the boundary of Ω) and two spheres centered at the conical point of radii $P > P^*$. See, for example, Fig. 13. Let us consider the weak formulation (37) over Ω^* , and particularly, let us examine the linear form $\mathcal{F}(\mathbf{v})$. Because homogeneous traction or displacement boundary conditions are considered, then $\mathcal{F}(\mathbf{v})$ is defined on the two spheres only. Using (35) and (41) we may rewrite (40) as

$$\mathbf{T} = \frac{1}{\rho} [n][E](\alpha [n]^T \mathbf{u} + [D^{(\theta,\phi)}] \mathbf{u}). \tag{42}$$

Substituting (42) in the linear form $\mathcal{F}(\mathbf{v})$ one obtains

$$\begin{aligned} \mathcal{F}(\mathbf{v}) &= P\alpha \iint_{\phi,\theta} [\mathbf{v}^T [n][E][n]^T \mathbf{u}]_P \sin \theta \, d\theta \, d\phi + P^*\alpha \iint_{\phi,\theta} [\mathbf{v}^T [n][E][n]^T \mathbf{u}]_{P^*} \sin \theta \, d\theta \, d\phi \\ &+ P \iint_{\phi,\theta} [\mathbf{v}^T [n][E][D^{(\theta,\phi)}] \mathbf{u}]_P \sin \theta \, d\theta \, d\phi + P^* \iint_{\phi,\theta} [\mathbf{v}^T [n][E][D^{(\theta,\phi)}] \mathbf{u}]_{P^*} \sin \theta \, d\theta \, d\phi. \end{aligned} \tag{43}$$

To simplify our notations we define

$$\mathcal{M}_P(\mathbf{u}, \mathbf{v}) \stackrel{\text{def}}{=} P \iint_{\phi,\theta} [\mathbf{v}^T [n][E][n]^T \mathbf{u}]_P \sin \theta \, d\theta \, d\phi \tag{44}$$

and

$$\mathcal{N}_P(\mathbf{u}, \mathbf{v}) \stackrel{\text{def}}{=} P \iint_{\phi,\theta} [\mathbf{v}^T [n][E][D^{(\theta,\phi)}] \mathbf{u}]_P \sin \theta \, d\theta \, d\phi \tag{45}$$

and with these notations the weak Steklov eigen-problem is

- **Seek** $\alpha \in \mathcal{C}$, $\mathbf{0} \neq \mathbf{u} \in [H^1(\Omega^*)]^3$ such that $\forall \mathbf{v} \in [H^1(\Omega^*)]^3$,

$$\mathcal{B}(\mathbf{u}, \mathbf{v}) - [\mathcal{N}_P(\mathbf{u}, \mathbf{v}) + \mathcal{N}_{P^*}(\mathbf{u}, \mathbf{v})] = \alpha [\mathcal{M}_P(\mathbf{u}, \mathbf{v}) + \mathcal{M}_{P^*}(\mathbf{u}, \mathbf{v})]. \tag{46}$$

Eq. (46) can be cast in a matrix form using the p -version of the finite element method. Because the conical point is excluded from the domain of analysis, the solution in this domain is regular up to the edges, and exponential convergence rate can be realized if the mesh is properly refined near edges.

5.1. Finite element discretization

We herein illustrate the steps needed to be followed to convert the bilinear form $\mathcal{B}(\mathbf{u}, \mathbf{v})$ into the stiffness matrix $[K]$, which we partition into nine blocks:

$$[K] \stackrel{\text{def}}{=} \begin{bmatrix} [K_{xx}] & [K_{xy}] & [K_{xz}] \\ [K_{xy}]^T & [K_{yy}] & [K_{yz}] \\ [K_{xz}]^T & [K_{yz}]^T & [K_{zz}] \end{bmatrix}. \quad (47)$$

The block $[K_{xx}]$, for example, can be expressed as

$$[K_{xx}] = \int_{P^*}^P \int_0^{\theta_o} \int_0^{2\pi} \mathbf{\partial}_{sp}^T v_x [Q]^T \begin{bmatrix} E_1 & E_7 & E_{16} \\ E_7 & E_{10} & E_{19} \\ E_{16} & E_{19} & E_{21} \end{bmatrix} [Q] \mathbf{\partial}_{sp} u_x \rho^2 \sin \theta \, d\rho \, d\theta \, d\phi, \quad (48)$$

where the transformation matrix $[Q]$ and the differentiation vector $\mathbf{\partial}_{sp}$ are given as

$$[Q] = \begin{bmatrix} \sin \theta \cos \phi & \frac{\cos \theta \cos \phi}{\rho} & \frac{-\sin \phi}{\rho \sin \theta} \\ \sin \theta \sin \phi & \frac{\cos \theta \sin \phi}{\rho} & \frac{\cos \phi}{\rho \sin \theta} \\ \cos \theta & \frac{-\sin \theta}{\rho} & 0 \end{bmatrix}, \quad \mathbf{\partial}_{sp} = \begin{Bmatrix} \partial_\rho \\ \partial_\theta \\ \partial_\phi \end{Bmatrix}. \quad (49)$$

The other five blocks $[K_{xy}]$, $[K_{xz}]$, $[K_{yy}]$, $[K_{yz}]$, and $[K_{zz}]$ are:

$$[K_{xy}] = \int_{P^*}^P \int_0^{\theta_o} \int_0^{2\pi} \mathbf{\partial}_{sp}^T v_x [Q]^T \begin{bmatrix} E_7 & E_2 & E_{11} \\ E_{10} & E_8 & E_{14} \\ E_{19} & E_{17} & E_{20} \end{bmatrix} [Q] \mathbf{\partial}_{sp} u_y \rho^2 \sin \theta \, d\rho \, d\theta \, d\phi,$$

$$[K_{xz}] = \int_{P^*}^P \int_0^{\theta_o} \int_0^{2\pi} \mathbf{\partial}_{sp}^T v_x [Q]^T \begin{bmatrix} E_{16} & E_{11} & E_4 \\ E_{19} & E_{14} & E_9 \\ E_{21} & E_{20} & E_{18} \end{bmatrix} [Q] \mathbf{\partial}_{sp} u_z \rho^2 \sin \theta \, d\rho \, d\theta \, d\phi,$$

$$[K_{yy}] = \int_{P^*}^P \int_0^{\theta_o} \int_0^{2\pi} \mathbf{\partial}_{sp}^T v_y [Q]^T \begin{bmatrix} E_{10} & E_8 & E_{14} \\ E_8 & E_3 & E_{12} \\ E_{14} & E_{12} & E_{15} \end{bmatrix} [Q] \mathbf{\partial}_{sp} u_y \rho^2 \sin \theta \, d\rho \, d\theta \, d\phi,$$

$$[K_{yz}] = \int_{P^*}^P \int_0^{\theta_o} \int_0^{2\pi} \mathbf{\partial}_{sp}^T v_y [Q]^T \begin{bmatrix} E_{19} & E_{14} & E_9 \\ E_{17} & E_{12} & E_5 \\ E_{20} & E_{15} & E_{13} \end{bmatrix} [Q] \mathbf{\partial}_{sp} u_z \rho^2 \sin \theta \, d\rho \, d\theta \, d\phi,$$

$$[K_{zz}] = \int_{P^*}^P \int_0^{\theta_o} \int_0^{2\pi} \mathbf{\partial}_{sp}^T v_z [Q]^T \begin{bmatrix} E_{21} & E_{20} & E_{18} \\ E_{20} & E_{15} & E_{13} \\ E_{18} & E_{13} & E_6 \end{bmatrix} [Q] \mathbf{\partial}_{sp} u_z \rho^2 \sin \theta \, d\rho \, d\theta \, d\phi.$$

The domain of interest Ω^* is partitioned into a small number of finite elements, with only one element in the radial direction. For example, Fig. 13 shows a finite element mesh containing 4 pentahedra elements for a conical point with an opening angle $\theta_o = 0.51\pi/2$.

Remark 8. For a purely conical vertex it is convenient to select a coordinate system with the z -axis along the cone axis, where z -axis points toward the body (the opposite as shown in Fig. 13). This way,

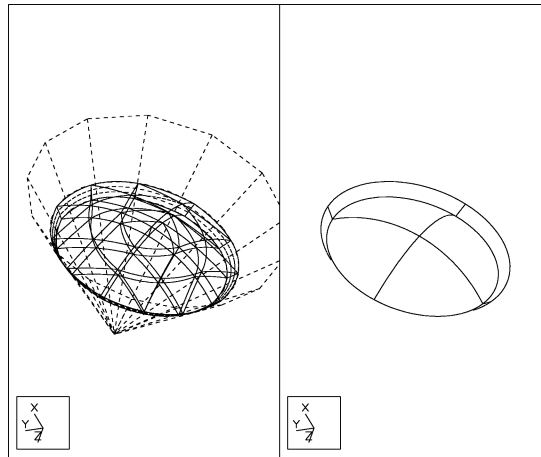


Fig. 13. Typical mesh for a 3-D rotationally symmetric conical vertex.

the limits of the integrals for the computation of the stiffness matrix terms are simply as provided herein. Otherwise, a change of coordinates is necessary.

6. Computing edge flux intensity functions for the Laplacian

Having computed the eigen-pairs, one may proceed to the computation of the edge flux/stress intensity functions or the vertex flux/stress intensity factors. We will demonstrate the procedure by extracting edge flux intensity functions (EFIFs) for the Laplace equation.

6.1. The dual weak form

Consider the edge subdomain $\mathcal{E}_{\delta,R}(\Lambda_{12})$ shown in Fig. 2. We define a vector space $E_c(\mathcal{E}_{\delta,R})$ as follows:

$$E_c(\mathcal{E}_{\delta,R}) = \left\{ \mathbf{q} \stackrel{\text{def}}{=} (q_x, q_y, q_z)^T \mid \iiint_{\mathcal{E}_{\delta,R}} |\mathbf{q}|^2 r \, d\theta \, dr \, dz < \infty, \operatorname{div} \mathbf{q} = \partial_x q_x + \partial_y q_y + \partial_z q_z = 0 \right\}. \quad (50)$$

We define by Γ_N that part of the boundary of $\mathcal{E}_{\delta,R}$ where $q_n = \partial q / \partial n = \hat{q}$ is prescribed. The space of admissible fluxes (for the Laplace operator) is denoted by $\tilde{E}_c(\mathcal{E}_{\delta,R})$ and is defined by

$$\tilde{E}_c(\mathcal{E}_{\delta,R}) = \{ \mathbf{q} \mid \mathbf{q} \in E_c(\mathcal{E}_{\delta,R}), q_n = \hat{q} \text{ on } \Gamma_N \}. \quad (51)$$

Note that if $\mathbf{q} = \operatorname{grad} u$, the condition $\operatorname{div} \mathbf{q} = 0$ is nothing more than the Laplace equation itself.

The dual weak form is stated as follows:

- Seek $\mathbf{q} \in \tilde{E}_c(\mathcal{E}_{\delta,R})$ such that

$$\mathcal{B}_c(\mathbf{q}, \mathbf{l}) = \mathcal{F}_c(\mathbf{l}) \quad \forall \mathbf{l} \in \tilde{E}_c(\mathcal{E}_{\delta,R}), \quad (52)$$

where

$$\mathcal{B}_c(\mathbf{q}, \mathbf{l}) \equiv \int_{r=0}^R \int_{\theta=0}^{\omega_{12}} \int_{z=z_1}^{z_2} \mathbf{q} \cdot \mathbf{l} r \, dr \, d\theta \, dz \quad (53)$$

and

$$\mathcal{F}_c(\mathbf{l}) \equiv \iint_{\Gamma_D} g_1(\mathbf{l} \cdot \mathbf{n}) \, dA. \quad (54)$$

Detailed discussion on the dual weak form and its relation to the primal weak form is given in [13]. To compute the edge flux intensity function associated with a particular eigen-pair by the dual weak formulation, one needs to generate a space of admissible fluxes.

6.2. Generating the space of admissible fluxes

For the two-dimensional Laplace equation over domains containing singularities this space is spanned by the eigen-pairs. In 3-D the situation is more complicated, and the space of admissible fluxes is considerably more difficult to be obtained. Once obtaining eigen-pairs for the 2-D Laplacian, one may proceed and construct admissible flux vectors for the 3-D Laplacian.

Let $r^\alpha f(\theta)$ be an eigen-pair of the two-dimensional Laplacian (denoted by Δ_{2D}) over the x - y plane perpendicular to an edge along the z -axis. Let $a(z)$ be the edge flux intensity function associated with the eigen-pair. Thus,

$$\Delta_{2D}[a(z)r^\alpha f(\theta)] = a(z)r^{\alpha-2}[\alpha^2 f(\theta) + f''(\theta)] = 0. \quad (55)$$

However, $a(z)r^\alpha f(\theta)$ does not satisfy the three dimensional Laplacian, $\Delta_{3D} = \Delta_{2D} + \partial_z^2$, where $\partial_z^2 \stackrel{\text{def}}{=} \partial^2/\partial z^2$.

$$\Delta_{3D}[a(z)r^\alpha f(\theta)] = \partial_z^2 a(z)r^\alpha f(\theta) \neq 0. \quad (56)$$

Augmenting the function $a(z)r^\alpha f(\theta)$ by

$$-\frac{1}{4(\alpha+1)}\partial_z^2 a(z)r^{\alpha+2} f(\theta)$$

then substituting in the Laplace equation, one obtains

$$\Delta_{3D}\left[a(z)r^\alpha f(\theta) - \frac{1}{4(\alpha+1)}\partial_z^2 a(z)r^{\alpha+2} f(\theta)\right] = -\frac{1}{4(\alpha+1)}\partial_z^4 a(z)r^{\alpha+2} f(\theta) \neq 0. \quad (57)$$

The edge flux intensity function is a smooth function of the variable z , so that it may be approximated by a basis of polynomials. Examining (57), one may notice that if $a(z)$ is a polynomial of degree smaller or equal to three then the two terms in (57) are a function from which an admissible flux can be obtained.

We may add a new function

$$\frac{1}{32(\alpha+1)(\alpha+2)}\partial_z^4 a(z)r^{\alpha+4} f(\theta),$$

so that now the residual is

$$\begin{aligned} \Delta_{3D}\left[a(z)r^\alpha f(\theta) - \frac{1}{4(\alpha+1)}\partial_z^2 a(z)r^{\alpha+2} f(\theta) + \frac{1}{32(\alpha+1)(\alpha+2)}\partial_z^4 a(z)r^{\alpha+4} f(\theta)\right] \\ = \frac{1}{32(\alpha+1)(\alpha+2)}\partial_z^6 a(z)r^{\alpha+4} f(\theta). \end{aligned} \quad (58)$$

The residual vanishes now if $a(z)$ is a polynomial of degree smaller or equal to five. We may proceed in a similar fashion, and obtain the following function $F_{\alpha,N}(r, \theta, z)$ associated with the 2-D eigen-pair $r^\alpha f(\theta)$:

$$F_{\alpha,N}(r, \theta, z) = r^\alpha f(\theta) \sum_{i=0}^N \partial_z^{2i} a(z) r^{2i} \frac{(-0.25)^i}{\prod_{j=1}^i j(\alpha + j)} \tag{59}$$

and the reminder is

$$\Delta_{3D} F_{\alpha,N} = \partial_z^{2N+2} a(z) r^{\alpha+2N} f(\theta) \frac{(-0.25)^N}{\prod_{j=1}^N j(\alpha + j)}. \tag{60}$$

It may be noticed that $F_{\alpha,N}(r, \theta, z)$ is indeed a function from which an admissible flux vector can be obtained, if $a(z)$ is a polynomial of order $2N + 1$ or smaller.

6.3. Computing the dual bi-linear form

Let $a_n(z)$ be the polynomial edge flux intensity function associated with the n th eigen-pair which may be represented by $\mathbf{P}^T(z)\mathbf{a}_n = \sum_{j=1}^{N+1} P_j(z)a_{nj}$. Here $P_j(z)$ are the ‘‘shape functions’’ based on integrals of Legendre polynomials defined in Section 4.1. The associated admissible flux vector is

$$\mathbf{q}_n = \left\{ \begin{matrix} \partial_x \\ \partial_y \\ \partial_z \end{matrix} \right\} u_n = \underbrace{\begin{bmatrix} \cos \theta & -\sin \theta & 0 \\ \sin \theta & \cos \theta & 0 \\ 0 & 0 & 1 \end{bmatrix}}_{[T]} \left\{ \begin{matrix} \partial_r \\ \frac{1}{r} \partial_\theta \\ r \partial_z \end{matrix} \right\} u_n. \tag{61}$$

Substituting (59) in (61) one obtains the admissible flux vector associated with the n th eigen-pair:

$$\mathbf{q}_n = [T] r^{\alpha_n-1} \mathbf{Q}_n \mathbf{a}_n, \tag{62}$$

where

$$\mathbf{Q}_n = \left\{ \begin{matrix} \alpha_n f_n(\theta) \mathbf{P}^T(z) - \frac{\alpha_n + 2}{4(\alpha_n + 1)} r^2 f_n(\theta) \partial_z^2 \mathbf{P}^T(z) + \frac{\alpha_n + 4}{32(\alpha_n + 1)(\alpha_n + 2)} r^4 f_n(\theta) \partial^4 \mathbf{P}^T(z) + \dots \\ f'_n(\theta) \mathbf{P}^T(z) - \frac{\alpha_n + 2}{4(\alpha_n + 1)} r^2 f'_n(\theta) \partial_z^2 \mathbf{P}^T(z) + \frac{\alpha_n + 4}{32(\alpha_n + 1)(\alpha_n + 2)} r^4 f'_n(\theta) \partial_z^4 \mathbf{P}^T(z) + \dots \\ r f_n(\theta) \partial_z \mathbf{P}^T(z) - \frac{\alpha_n + 2}{4(\alpha_n + 1)} r^3 f_n(\theta) \partial_z^3 \mathbf{P}^T(z) + \frac{\alpha_n + 4}{32(\alpha_n + 1)(\alpha_n + 2)} r^5 f_n(\theta) \partial_z^5 \mathbf{P}^T(z) + \dots \end{matrix} \right\}^T.$$

Similarly, we construct the admissible flux vector associated with the m th eigen-pair $\mathbf{l}_m = [T] \mathbf{Q}_m \mathbf{a}_m$, so that

$$\mathbf{q}_n^T \cdot \mathbf{l}_m = \mathbf{a}_n^T \mathbf{Q}_n^T [T]^T [T] \mathbf{Q}_m \mathbf{a}_m = \mathbf{a}_n^T \mathbf{Q}_n^T \mathbf{Q}_m \mathbf{a}_m. \tag{63}$$

If homogeneous boundary conditions are applied on the faces $\theta = 0$ and $\theta = \omega_{12}$ of the domain $\mathcal{E}_{\delta,R}$, then one can show that $\int_{\theta=0}^{\omega_{12}} f_n(\theta) f_m(\theta) d\theta = 0$ for $n \neq m$ (orthogonality of the eigen-functions), $\int_{\theta=0}^{\omega_{12}} f'_n(\theta) f'_m(\theta) d\theta = 0$ for $n \neq m$ and

$$\int_{\theta=0}^{\omega_{12}} [f'_n(\theta)]^2 d\theta = \alpha_n^2 \int_{\theta=0}^{\omega_{12}} [f_n(\theta)]^2 d\theta.$$

With this in mind, and after substituting (63) in the expression for the dual bilinear form (52), one obtains

$$\mathcal{B}_c(\mathbf{q}_n, \mathbf{l}_m) = 0 \quad \text{for } n \neq m \tag{64}$$

and

$$\begin{aligned} \mathcal{B}_c(\mathbf{q}_n, \mathbf{l}_n) = & \mathbf{a}_n^T \int_{\theta=0}^{\omega_1^2} [f_n(\theta)]^2 d\theta \left\{ \alpha_n R^{2\alpha_n} \Delta z [PP] \right. \\ & + \frac{R^{2(\alpha_n+1)}}{\Delta z (\alpha_n + 1)} \left([DPDP] - \frac{\alpha_n}{2} ([PD^2P] + [PD^2P]^T) \right) \\ & + \frac{R^{2(\alpha_n+2)}}{(\Delta z)^3 (\alpha_n + 1)(\alpha_n + 2)} \left(\frac{\alpha_n^2 + \alpha_n + 2}{2(\alpha_n + 1)} [D^2PD^2P] - ([DPD^3P] + [DPD^3P]^T) \right) \\ & \left. + \frac{R^{2(\alpha_n+3)}}{(\Delta z)^5 (\alpha_n + 1)^2 (\alpha_n + 3)} [D^3PD^3P] + \dots \right\} \mathbf{a}_n. \end{aligned} \tag{65}$$

The above expression for the dual bilinear form is exact for $a_n(z)$ being polynomials up to degree five. Otherwise the next term which is missing is of order $O(R^{2(\alpha_n+4)})$, and the fifth–seventh rows and columns are required in the matrices given as follows:

$$\begin{aligned} [PP] = & \begin{bmatrix} \frac{2}{3} & \frac{1}{3} & \frac{-1}{\sqrt{6}} & \frac{1}{3\sqrt{10}} & \dots \\ & \frac{2}{3} & \frac{-1}{\sqrt{6}} & \frac{-1}{3\sqrt{10}} & \dots \\ & & \frac{2}{5} & 0 & \dots \\ \text{[SYM]} & & & \frac{2}{21} & \dots \end{bmatrix}, & [DPDP] = & \begin{bmatrix} \frac{1}{2} & \frac{-1}{2} & 0 & 0 & \dots \\ & \frac{1}{2} & 0 & 0 & \dots \\ & & 1 & 0 & \dots \\ \text{[SYM]} & & & 1 & \dots \end{bmatrix}, \\ [PD^2P] = & \begin{bmatrix} 0 & 0 & \sqrt{\frac{3}{2}} & -\sqrt{\frac{10}{2}} & \dots \\ 0 & 0 & \sqrt{\frac{3}{2}} & \sqrt{\frac{10}{2}} & \dots \\ 0 & 0 & -1 & 0 & \dots \\ 0 & 0 & 0 & -1 & \dots \end{bmatrix}, & [D^2PD^2P] = & \begin{bmatrix} 0 & 0 & 0 & 0 & \dots \\ & 0 & 0 & 0 & \dots \\ & & 3 & 0 & \dots \\ \text{[SYM]} & & & 15 & \dots \end{bmatrix}, \\ [DPD^3P] = & \begin{bmatrix} 0 & 0 & 0 & -\frac{30}{2\sqrt{10}} & \dots \\ 0 & 0 & 0 & \frac{30}{2\sqrt{10}} & \dots \\ 0 & 0 & 0 & 0 & \dots \\ 0 & 0 & 0 & 0 & \dots \end{bmatrix}, & [D^3PD^3P] = & \begin{bmatrix} 0 & 0 & 0 & 0 & \dots \\ & 0 & 0 & 0 & \dots \\ & & 0 & 0 & \dots \\ \text{[SYM]} & & & 90 & \dots \end{bmatrix}. \end{aligned}$$

In (65) $\Delta z = z_2 - z_1$ is the length of the cylindrical sector over which the dual weak form is computed. The “compliance matrix” associated with \mathcal{B}_c is a block diagonal matrix, with each block of size $N + 1$ (N being the order of polynomial approximation of the eigen-functions).

6.4. Computing the dual linear form

The dual linear form $\mathcal{F}_c(\mathbf{l})$ is defined on the surface of the cylindrical sector shown in Fig. 2. Because we assume homogeneous boundary conditions on the two planes intersecting at the edge of interest, the

linear form vanishes on them. Let us consider first the linear form associated with the n th eigen-pair over the cylindrical surface, denoted by $[\mathcal{F}_c(\mathbf{l}_n)]_{\text{cyl}}$:

$$\begin{aligned}
 [\mathcal{F}_c(\mathbf{l}_n)]_{\text{cyl}} &= \int_0^{\omega_{12}} \int_{z_1}^{z_2} u(R, \theta, z) \left[\alpha_n R^{\alpha_n-1} f_n(\theta) \left(\mathbf{P}^T(z) - \frac{\alpha_n + 2}{4(\alpha_n + 1)} R^2 \partial_z^2 \mathbf{P}^T(z) \right. \right. \\
 &\quad \left. \left. + \frac{\alpha_n + 4}{32(\alpha_n + 1)(\alpha_n + 2)} R^4 \partial_z^4 \mathbf{P}^T(z) + \dots \right) \right] \mathbf{a}_n R \, d\theta \, dz \\
 &= \left\{ \frac{\alpha_n \Delta z}{2} R^{\alpha_n} \int_0^{\omega_{12}} \int_{-1}^1 u(R, \theta, \zeta) f_n(\theta) \mathbf{P}^T(\zeta) \, d\theta \, d\zeta \right. \\
 &\quad \left. - \frac{\alpha_n + 2}{2\Delta z(\alpha_n + 1)} R^{\alpha_n+2} \int_0^{\omega_{12}} \int_{-1}^1 u(R, \theta, \zeta) f_n(\theta) \left(0, 0, \sqrt{\frac{3}{2}}, \frac{3\sqrt{10}\zeta}{2}, \dots \right) \, d\theta \, d\zeta \right\} \mathbf{a}_n. \quad (66)
 \end{aligned}$$

Remark 9. Note that the above expressions are based on the assumption that the edge flux intensity functions are polynomials of at most degree three. Otherwise, more terms are required to be accounted for. However, since the edge flux intensity function are smooth, and an adaptive selection of an increasing order of polynomials is considered one can decide whether a higher polynomial order is required.

There are two more planes over which the dual linear form is defined. These are the top and bottom faces of the cylinder. The dual linear form for $z = z_1$ is

$$\begin{aligned}
 [\mathcal{F}_c(\mathbf{l}_n)]_{z_1} &= \left\{ -\frac{\Delta z}{2} \int_0^{\omega_{12}} \int_0^R u(r, \theta, z_1) r^{\alpha_n+1} f_n(\theta) \, dr \, d\theta \left(\frac{-1}{2}, \frac{1}{2}, -\sqrt{\frac{6}{4}}, \sqrt{\frac{10}{4}}, \dots \right) \right. \\
 &\quad \left. + \frac{(\Delta z)^3}{32(\alpha_n + 1)} \int_0^{\omega_{12}} \int_0^R u(r, \theta, z_1) r^{\alpha_n+3} f_n(\theta) \, dr \, d\theta \left(0, 0, 0, \frac{30}{2\sqrt{10}}, \dots \right) \right\} \mathbf{a}_n, \quad (67)
 \end{aligned}$$

and for the plane $z = z_2$:

$$\begin{aligned}
 [\mathcal{F}_c(\mathbf{l}_n)]_{z_2} &= \left\{ \frac{\Delta z}{2} \int_0^{\omega_{12}} \int_0^R u(r, \theta, z_2) r^{\alpha_n+1} f_n(\theta) \, dr \, d\theta \left(\frac{-1}{2}, \frac{1}{2}, -\sqrt{\frac{6}{4}}, \sqrt{\frac{10}{4}}, \dots \right) \right. \\
 &\quad \left. - \frac{(\Delta z)^3}{32(\alpha_n + 1)} \int_0^{\omega_{12}} \int_0^R u(r, \theta, z_2) r^{\alpha_n+3} f_n(\theta) \, dr \, d\theta \left(0, 0, 0, \frac{30}{2\sqrt{10}}, \dots \right) \right\} \mathbf{a}_n. \quad (68)
 \end{aligned}$$

Adding (66)–(68) provides the “load vector” (with $N + 1$ elements) associated with the n th eigen-pair. We then assemble the load vectors for the number of edge flux intensity functions of interest to obtain the right-hand side of (52). Notice that the exact function u in (66)–(68) is not known, so that we use its finite element approximation. The left-hand side of (52) is the compliance matrix given by (65), so that all which is left is the solution of a symmetric system of equations.

7. Summary and conclusions

This paper addresses numerical methods for computing singular solutions of linear second order elliptic partial differential equations (Laplace and Elasticity problems) in polyhedra domains, using the p -version of the finite element method. Specifically, we have addressed singularities associated with straight edges and vertices, and concentrate our attention on the computation of eigen-pairs by the weak modified Steklov eigen-formulation. This formulation has been presented for both the Laplace and elasticity problems, and a numerical example provided. The method has several advantages, namely, it is general for two-dimensional and three-dimensional domains and has been shown to be both accurate, reliable and super-convergent in two-dimensions [22] as well as for edge singularities in three-dimensions. Its implementation for 3-D vertex singularities is in progress and numerical results will be presented in the future.

By using the computed eigen-pairs, and the dual weak formulation, a method has been presented for extracting the edge flux intensity functions for the Laplace problem. This is a post-solution operation on the finite element solution vector. An adaptive strategy of selecting an increasing order of polynomials to approximate the edge flux intensity functions together with the hierarchical space of the p -version finite element method is expected to provide an optimal convergence rate. The method is being implemented and numerical examples will be presented in a forthcoming paper.

Acknowledgements

The author would like to thank Profs. Martin Costabel and Monique Dauge of University of Rennes 1, France, for their valuable comments on the space of admissible fluxes. The reported work has been partially supported by the AFOSR under STTR/TS project No. F-49620-97-C-0045.

References

- [1] B. Andersson, U. Falk, I. Babuška, T. Von-Petersdorff, Reliable stress and fracture mechanics analysis of complex components using a h-p version of FEM, *Internat. J. Numer. Methods Engrg.* 38 (1995) 2135–2163.
- [2] I. Babuška, A.K. Aziz, Survey lectures on the mathematical foundations of the finite element method, in: A.K. Aziz (Ed.), *The Mathematical Foundations of the Finite Element Method with Applications to Partial Differential Equations*, Academic Press, New York, 1972, pp. 3–343.
- [3] I. Babuška, T. Von-Petersdorff, B. Andersson, Numerical treatment of vertex singularities and intensity factors for mixed boundary value problems for the Laplace equation in \mathbb{R}^3 , *SIAM J. Numer. Anal.* 31 (5) (1994) 1265–1288.
- [4] A. Beagles, A.-M. Sändig, Singularities of rotationally symmetric solutions of boundary value problems for the Lamé equations, *Z. Angew. Math. Mech.* 71 (1991) 423–431.
- [5] M. Costabel, M. Dauge, Computation of corner singularities in linear elasticity, in: M. Costabel, M. Dauge and S. Nicaise (Eds.), *Boundary Value Problems and Integral Equations in Nonsmooth Domains*, Marcel Dekker, New York; Basel, Hong-Kong, 1995, pp. 59–68.
- [6] M. Costabel, M. Dauge, General edge asymptotics of solution of second order elliptic boundary value problems I & II, *Proc. Roy. Soc. Edinburgh Sect. A* 123 (1993) 109–184.
- [7] M. Costabel, M. Dauge, Y. Lafranche, Fast semi-analytic computation of elastic edge singularities, Preprint, submitted for publication, 1998.

- [8] M. Dauge, *Elliptic Boundary Value Problems in Corner Domains—Smoothness and Asymptotics of Solutions*, Lecture Notes in Mathematics, Vol. 1341, Springer-Verlag, Heidelberg, 1988.
- [9] P. Grisvard, *Singularities in Boundary Value Problems*, Masson, France, 1992.
- [10] B. Guo, H-S. Oh, The method of auxiliary mapping for the finite element solutions of elliptic partial differential equations on nonsmooth domains in \mathbb{R}^3 , Preprint, Math. Comp. (1996, submitted).
- [11] L. Gu, T. Belytschko, A numerical study of stress singularities in a two-material wedge, *Internat. J. Solids Structures* 31 (6) (1994) 865–889.
- [12] D. Leguillon, E. Sanchez-Palencia, *Computation of Singular Solutions in Elliptic Problems and Elasticity*, Wiley, New York, 1987.
- [13] J.T. Oden, J.N. Reddy, *Variational Methods in Theoretical Mechanics*, Springer-Verlag, New-York, 1983.
- [14] S.S. Pageau, S.B. Jr. Biggers, A finite element approach to three dimensional singular stress states in anisotropic multi-material wedges and junctions, *Internat. J. Solids Structures* 33 (1996) 33–47.
- [15] B.A. Szabó, I. Babuška, *Finite Element Analysis*, Wiley, New York, 1991.
- [16] B.A. Szabó, Z. Yosibash, Numerical analysis of singularities in two-dimensions, Part 2: Computation of the generalized flux/stress intensity factors, *Internat. J. Numer. Methods Engrg.* 39 (3) (1996) 409–434.
- [17] B.A. Szabó, Z. Yosibash, Superconvergent computations of flux intensity factors and first derivatives by the FEM, *Comput. Methods Appl. Mech. Engrg.* 129 (4) (1996) 349–370.
- [18] T.C.T. Ting, S.C. Chou, Edge singularities in anisotropic composites, *Internat. J. Solids Structures* 17 (11) (1981) 1057–1068.
- [19] S.S. Wang, I. Choi, Boundary layer effects in composite laminates: Part 1—free edge stress singularities, *Trans. ASME, J. Appl. Mech.* 49 (1982) 541–548.
- [20] Z. Yosibash, Numerical analysis of edge singularities in three-dimensional elasticity, *Internat. J. Numer. Methods Engrg.* 40 (1997) 4611–4632.
- [21] Z. Yosibash, Computing edge singularities in elastic anisotropic three-dimensional domains, *Internat. J. Fracture* 86 (3) (1997) 221–245.
- [22] Z. Yosibash, B.A. Szabó, Numerical analysis of singularities in two-dimensions, Part 1: Computation of eigenpairs, *Internat. J. Numer. Methods Engrg.* 38 (12) (1995) 2055–2082.
- [23] Z. Yosibash, B.A. Szabó, Generalized stress intensity factors in linear elastostatics, *Internat. J. Fracture* 72 (3) (1995) 223–240.